Variational Data Assimilation in the Tropics Using Precipitation Data. Part III: Assimilation of SSM/I Precipitation Rates

TADASHI TSUYUKI*

Department of Meteorology, The Florida State University, Tallahassee, Florida

(Manuscript received 28 May 1996, in final form 16 October 1996)

ABSTRACT

The performance of four-dimensional variational data assimilation (4D-VAR) in the Tropics is examined by assimilating radiosonde and pibal data over the globe and Special Sensor Microwave/Imager (SSM/I) precipitation rates over the tropical oceans for the period 0000–1200 UTC 22 August 1992. The cost function consists of a discrepancy term between model and observations and a penalty term for suppressing gravity wave noise. The assimilation model (forward model) is a full-physics global spectral model, while physics of the adjoint model only includes moist processes, horizontal diffusion, and simplified surface friction. Several types of discontinuity are removed from the parameterizations of the moist processes.

It is found that the following three procedures improve the convergence performance of 4D-VAR in which the adjoint model includes moist processes: appropriate control of gravity wave level, removal of discontinuities from the parameterization schemes of the moist processes, and use of a higher-order horizontal interpolation operator for precipitation when assimilating precipitation data. 4D-VAR, using the adjoint model that lacks the moist processes, produces a poor analysis in the Tropics despite the fact that the full-physics model is used as the forward model. Inclusion of the moist processes in the adjoint model leads to a better precipitation analysis even without assimilating the SSM/I precipitation rates, especially in areas where several radiosonde and pibal observations are available. However, the convergence rate is slightly decelerated by including the moist processes. The impact of assimilating SSM/I precipitation rates on the precipitation analysis is not confined to near SSM/I observation times but spreads over the whole assimilation window. Its impact on the precipitable water analysis over the tropical oceans is positive but very small, suggesting the necessity of assimilating satellite precipitable water data. Assimilation of the SSM/I precipitation rates slightly improves the precipitation forecast over the tropical oceans.

An implication of the results for the Tropical Rainfall Measuring Mission (TRMM) project is discussed.

1. Introduction

Four-dimensional variational data assimilation (4D-VAR) is one of the advanced data assimilation methods to which considerable attention has been paid in recent years. 4D-VAR is a comprehensive multivariate analysis technique using model dynamics and imposes no limitation on the type of data to be assimilated. Application of 4D-VAR to the dynamics of the extratropical atmosphere has demonstrated its several advantages over conventional optimal interpolation (OI) methods (e.g., Thépaut et al. 1993a,b; Andersson et al. 1994). Since global models used in the above studies did not include moist processes that play the primary role in determining tropical large-scale circulations, application of 4D-VAR to the tropical atmosphere has not been well examined. Introduction of moist processes into 4D-VAR had been considered difficult due to strong nonlinearities in the parameterization of moist processes, especially discontinuous threshold processes included in the parameterization schemes. However, Zou et al. (1993b) demonstrated the ability to perform 4D-VAR with discontinuous physical processes. D. Zupanski (1993) showed that the adverse effects of discontinuities in a cumulus convection scheme can be reduced by modifying the scheme to make it more continuous. Their results encouraged development of 4D-VAR with physical processes and its application to tropical data analysis.

The major advantage of 4D-VAR in the Tropics is the use of full model dynamics to assimilate observational data. Geostrophic balance is not a reasonable approximation for the flow in synoptic-scale tropical systems. As a result, it is difficult to improve the wind analysis from temperature observations and vice versa in conventional OI procedures. The geopotential and wind fields are usually analyzed univariately in the Tropics. A more appropriate balance relationship for

*On leave from the Japan Meteorological Agency, Tokyo, Japan.

Corresponding author address: Tadashi Tsuyuki, Numerical Prediction Division, Japan Meteorological Agency, 1-3-4 Ote-machi, Chiyoda-ku, Tokyo 100, Japan.
E-mail: tsuyuki@npd.kishou.go.jp

tropical multivariate data analysis can be derived under certain conditions. A scale analysis of synoptic-scale circulations in which the vertical scale is comparable to the scale height of the atmosphere shows that in the absence of condensation heating or precipitating systems the flow in the Tropics is nearly nondivergent (Holton 1992). Absolute vorticity is approximately conserved following the nondivergent wind, and the following diagnostic relationship between the geopotential Φ and streamfunction Ψ can be derived from the divergence equation:

$$\nabla^2\left[\Phi + \frac{1}{2}(\nabla\Psi)^2\right] = \nabla\cdot[(f + \nabla^2\Psi)\nabla\Psi], \qquad (1)$$

where f is the Coriolis parameter, ∇ the horizontal gradient operator, and ∇^2 the horizontal Laplacian operator. This nonlinear balance equation can be introduced as a weak constraint in three-dimensional variational data assimilation (3D-VAR) procedures. For synoptic-scale precipitating systems in the Tropics, however, the average vertical motion is an order of magnitude larger than the vertical motion in nonprecipitating areas. Consequently, the flow in these systems has a relatively large divergent component so that the barotropic vorticity equation is no longer a good approximation. The primitive equations must be applied to analyze the flow. The OI and 3D-VAR procedures face an intrinsic limitation for this purpose. 4D-VAR uses the primitive equations to assimilate observational data and, therefore, is quite appropriate for tropical data assimilation.

The success of physical initialization proposed by Krishnamurti et al. (1984) in improving the forecast skill of tropical numerical weather prediction (NWP) suggested potential benefits from assimilating precipitation data in the Tropics. Assimilation of precipitation data with 4D-VAR was first tried by Zupanski and Mesinger (1995) using a midlatitude regional model. Advantages of 4D-VAR over physical initialization in assimilating precipitation data were pointed out in the introduction of Tsuyuki (1996b), hereafter referred to as Part II. Available sources of precipitation data include rain gauge observations, rain radar observations, and estimates derived from satellite observations by various techniques. Since the spatial distribution of the former two sources is generally limited to populated land areas, satellites estimates are the primary data source for precipitation over the global Tropics. Satellite infrared (IR) data are available from geostationary satellites, thereby permitting nearly continuous sampling in time. IR-based precipitation estimates include the GOES precipitation index (GPI) of Arkin and Meisner (1987) and the convective–stratiform technique (CST) of Adler and Negri (1988). The indirect nature of the relationship between IR observations and precipitation has limited the success of the IR techniques. Satellite microwave data, especially from the Special Sensor Microwave/Imager (SSM/I) on polar-orbiting satellites in the U.S. Defense Meteorological Satellite Program (DMSP), provide more direct information on precipitation. Although microwave estimates of precipitation are more accurate than IR estimates, they are available only a few times a day from polar-orbiting platforms. At this time microwave sensors cannot be made compact enough to provide sufficient resolution from a geosynchronous orbit. Several algorithms for retrieving precipitation rates from SSM/I brightness temperature have been proposed (e.g., Olson 1989; Kidd and Barrett 1990; Grody 1991; Adler et al. 1991; Wilheit et al. 1991; Berg and Chase 1992; Liu and Curry 1992; Kumerrow and Giglio 1994a,b; Petty 1994a,b). 4D-VAR is capable of assimilating asynoptic satellite data such as microwave estimates of precipitation in a straightforward way.

However, there is a difficulty in applying 4D-VAR to tropical data assimilation. In contrast to the extratropical atmosphere, cumulus convection plays a dominant role in determining large-scale atmospheric flow in the Tropics. This property makes it essential to include parameterization of cumulus convection in 4D-VAR. Since the physics is far more nonlinear than the dynamics, the tangent-linear approximation is less valid for a model with physics than for the same model without physics. In particular, threshold processes in parameterization schemes make a cost function discontinuous or nondifferentiable. These strong nonlinearities degrade the efficiency of commonly used minimization algorithms. This is one of the problems to solve for applying 4D-VAR to tropical data assimilation.

This paper is the third part of the author's study on the feasibility of 4D-VAR in the Tropics using precipitation data. The first part (Tsuyuki 1996a), hereafter referred to as Part I, presented a basic formulation of 4D-VAR using precipitation data, removal of several types of discontinuity from parameterized moist processes to improve convergence performance, and results from assimilation experiments with a column model. The results showed that variational data assimilation with discontinuous moist processes exhibits poor convergence properties and large analysis errors. In the second part (Part II), a global primitive equation model was used to examine the performance of 4D-VAR in the Tropics and to assess the impact of assimilating precipitation data. Truth and observations were provided by a simulation run using a full-physics model, while the assimilation model (forward model) and the adjoint model only included moist processes, horizontal diffusion, and simplified surface friction. It was found that despite the fact that wind observations in the Tropics were assumed to be available at only two levels, the wind analysis error was decreased from the initial guess error at all model levels without using specific vertical structure functions. A penalty term for suppressing gravity wave noise increased the efficiency of 4D-VAR with moist processes by avoiding locally large gradients in the cost function during the minimization process. 4D-VAR with the moist processes yielded a better anal-

ysis of divergence, moisture, and lower-tropospheric vorticity in the Tropics despite a slower convergence rate than 4D-VAR without the moist processes. The moisture analysis error in the lower troposphere decreased from the initial guess without assimilating moisture observations. Further improvements resulted from assimilating precipitation data. However, major improvements were generally confined to areas of heavy precipitation.

The results from Part I and Part II strongly suggested that 4D-VAR is possible in the Tropics. Furthermore, the results indicated several advantages of 4D-VAR over OI and 3D-VAR in tropical data assimilation. These results, however, were obtained in a simulated data framework. Assimilation experiments using real observational data are necessary to further evaluate the feasibility of 4D-VAR in the Tropics. In this third part, radiosonde and pibal data over the globe and SSM/I precipitation rates over the tropical oceans are assimilated. Radiosonde and pibal data are major observational data even in the Tropics. For the purpose of examining the performance of 4D-VAR in the Tropics, assimilation of asynoptic satellite data such as the SSM/I estimates for precipitation rates may be more appropriate than assimilation of synoptic satellite data such as IR estimates from geostationary satellites. Direct assimilation of SSM/I measurements of microwave brightness temperature may be better than assimilating precipitation rates retrieved from the SSM/I brightness temperature. However, the direct assimilation requires prediction of cloud water and rainwater, as well as a microwave radiative transfer model. This approach is not taken in the present study.

The purposes of this paper are threefold: to examine how 4D-VAR works in the Tropics, to demonstrate the importance of moist processes in the tropical data assimilation, and to assess the impact of assimilating SSM/I precipitation rates. As mentioned in Part II, preconditioning and systematic error correction are desirable for a faster convergence rate and better quality of the resulting analyses, but these procedures are not introduced for the sake of simplicity. Since a background term that measures discrepancy between model and an initial guess is not included in the cost function as in Part I and Part II, a comparison with operational analyses is not intended here. In operational analyses information obtained from the previous analysis cycle is effectively utilized as the first guess. A 4D-VAR formulation without a background term makes it difficult to utilize this information. As a result, the quality of analyses produced from the assimilation experiments performed here may be worse than the quality of operational analyses.

This manuscript is organized as follows. The design of the assimilation experiments and an outline of the model are given in section 2. Section 3 is devoted to a description of the radiosonde and pibal data and the SSM/I precipitation rates assimilated in the experiments. Section 4 presents results of the experiments, including 72-h forecast experiments and the sensitivity of 4D-VAR convergence performance to the penalty parameter, the horizontal interpolation operator, and discontinuities in parameterization schemes of the moist processes. Conclusions are summarized in section 5.

2. Method

The model state variables at all time levels in the assimilation window, $\mathbf{x}$, are determined by the model $\mathbf{F}$ and the initial condition $\mathbf{x}_0$:

$$\mathbf{x} = \begin{pmatrix} \mathbf{x}_0 \\ \mathbf{x}_1 \\ \vdots \\ \mathbf{x}_N \end{pmatrix} = \mathbf{F}(\mathbf{x}_0), \tag{2}$$

where the subscripts indicate time levels and $N + 1$ is the total number of time levels in the assimilation window. The cost function used here is similar to that used in Part II. The cost function consists of a discrepancy term between model and observations and a penalty term for suppressing gravity wave noise and does not include a background term:

$$J(\mathbf{x}_0) = \frac{1}{2}[\mathbf{H}(\mathbf{x}) - \mathbf{y}]^{\mathrm{T}}\mathbf{O}^{-1}[\mathbf{H}(\mathbf{x}) - \mathbf{y}] + \frac{1}{2}r\left(\frac{\partial \mathbf{D}}{\partial t}\right)^{\mathrm{T}}\mathbf{W}\frac{\partial \mathbf{D}}{\partial t}, \tag{3}$$

where the superscript T indicates the transpose of vectors or matrices. In the first term on the right-hand side, $\mathbf{y}$ is the observations available in the assimilation window, $\mathbf{H}$ is the observation operator that converts the model state variables to observed variables and interpolates from model grid points to observation points, and $\mathbf{O}$ is the observation error covariance matrix. The second term is the penalty term that controls the magnitude of the global mean of the squared divergence time tendency. Term r denotes the penalty parameter, $\partial\mathbf{D}/\partial t$ is the time tendency of model divergence at all time levels, and $\mathbf{W}$ is a positive-definite symmetric matrix consisting of weights to calculate the global mean. This simple penalty term to suppress gravity wave noise was first introduced into 4D-VAR by Zou et al. (1993a). The gradient of the cost function with respect to the initial condition is written as follows:

$$\nabla_{\mathbf{x}_0} J = \left(\frac{\partial \mathbf{F}}{\partial \mathbf{x}_0}\right)^{\mathrm{T}}\left\{\left(\frac{\partial \mathbf{H}}{\partial \mathbf{x}}\right)^{\mathrm{T}}\mathbf{O}^{-1}[\mathbf{H}(\mathbf{x}) - \mathbf{y}] + r\left(\frac{\partial}{\partial \mathbf{x}}\frac{\partial \mathbf{D}}{\partial t}\right)^{\mathrm{T}}\mathbf{W}\frac{\partial \mathbf{D}}{\partial t}\right\}. \tag{4}$$

The transpose of the Jacobian matrix of the model on the right-hand side represents the adjoint model. The adjoint model is integrated backward in time to calculate the gradient.

The model is a low-resolution version of the Florida State University global spectral model (FSU GSM). It

has a horizontal resolution of triangular truncation at total wavenumber 42 with 12 levels in the vertical (T42L12). The number of Gaussian grid points is 64 (latitude) $\times$ 128 (longitude). The vertical coordinate is sigma, defined as

$$\sigma = \frac{p}{p_s}, \tag{5}$$

where p is the pressure and p_s is the surface pressure. The model state variables are vorticity, divergence, virtual temperature, dewpoint depression, and the logarithm of surface pressure. The former three variables are defined at all model levels, while dewpoint depression is defined only at the lowest 10 levels. The time step is 1200 s. The physics includes radiation (Chang 1979), surface fluxes (Businger et al. 1971), planetary boundary layer, vertical diffusion (Louis 1979), horizontal diffusion, dry convective adjustment, large-scale condensation and evaporation, and deep cumulus convection. The latter three physical processes are referred to as the moist processes in this paper. A modified Kuo scheme is used for parameterization of deep cumulus convection (Krishnamurti et al. 1983). For a detailed description of the FSU GSM see Pasch (1983). In the present study several types of discontinuity are removed from the original parameterization schemes of the moist processes in order to improve the convergence properties of 4D-VAR. A detailed discussion of the modifications to the original parameterization schemes is given in Part I. The physics of the adjoint model includes the moist processes, horizontal diffusion, and simplified surface friction. This package of physics is hereafter referred to as the reduced physics.

The 12-h period of 0000–1200 UTC 22 August 1992 is chosen as the assimilation window. As will be mentioned in section 3b, the SSM/I precipitation rates do not entirely cover the tropical oceans during this 12-h period. Increasing the length of the assimilation window is possible, but the adverse effects of model error on 4D-VAR will also increase. The nonlinear normal-mode initialization with physics (Kitade 1983) is applied to the National Centers for Environmental Prediction (NCEP) operational analysis at the beginning of the assimilation window (0000 UTC 22 August 1992). This initialized analysis serves as the initial guess for the model state at the same point. Different from Part II, the full-physics model is used as the forward model. Since the 4D-VAR formulation adopted here assumes that the model is perfect, the full-physics model may be more appropriate as the forward model when assimilating real observations. In this case, however, the adjoint model with the reduced-physics does not produce exact gradients of the cost function. Such a procedure has already been adopted by M. Zupanski (1993) and Zupanski and Mesinger (1995). They showed that this procedure produced better analyses than another procedure in which the reduced-physics model consistent with the adjoint model is used as the forward model. The reason why this procedure was not adopted in Part II, in which simulated data were assimilated, was because overly optimistic results were obtained if the same model was used to both generate and assimilate the simulated data. As in Part II, three assimilation methods are compared to assess the importance of moist processes for 4D-VAR in the Tropics and to evaluate the benefits of assimilating precipitation data. The first method, hereafter referred to as NOMP, uses the adjoint model that lacks the moist processes. The second method, hereafter referred to as MP, uses the adjoint model with the moist processes included but does not assimilate the SSM/I precipitation rates. The third method, hereafter referred to as MP+RR, uses the same adjoint model as in MP but assimilates the SSM/I precipitation rates.

In this study the minimization is performed in spectral space in contrast to Part II where the control variables were defined in physical space. Minimization in spectral space may be more appropriate because the model is a spectral model and this procedure requires much less memory. A preliminary experiment using a 1-h assimilation window showed that there was no significant difference in convergence performance between minimizations in spectral space and physical space. The L-BFGS method (Liu and Nocedal 1989) is applied to minimize the cost function. The quasi-Newton approximation of the inverse Hessian matrix is updated using information from the last five quasi-Newton iterations. The maximum numbers of iterations and function calls are set to 30 and 40, respectively. One function call consists of one forward integration of the assimilation model and one backward integration of the adjoint model. One iteration of the unconstrained minimization algorithm sometimes requires more than one function call due to the line search.

Scaling factors for the control variables are 10^{-5} s^{-1} for the vorticity and divergence, 1 K for the virtual temperature, 2 K for the dewpoint depression, and 10^{-3} for the logarithm of surface pressure. These scaling factors are not optimized to yield a faster convergence rate. They are the same as those used in Part II except that the inverse square roots of the Gaussian weights are not multiplied. Multiplication by the inverse square roots was introduced in Part II because the observations were provided on the model Gaussian grid and the cost function was defined in terms of the global integral rather than a summation over the Gaussian grid points.

3. Observational data

a. Radiosonde and pibal data

Radiosonde and pibal data for 0000–1200 UTC 22 August 1992 are taken from the NCEP upper-air data subsets archived at the National Center for Atmospheric Research (NCAR). These data represent what NCEP

TABLE 1. Observation error standard deviations for assimilated radiosonde and pibal data.

Level (hPa)	Geopotential height (gpm)	Wind (m s^{-1})	Temperature (K)	Relative humidity (%)
100	—	2.5	3.1	—
150	—	3.0	2.8	—
200	—	3.3	2.5	—
250	—	3.4	2.2	—
300	—	3.4	2.0	20
400	—	3.1	1.6	20
500	—	2.8	1.3	20
700	—	2.4	1.3	20
850	—	2.0	1.5	20
1000	7.0	1.4	1.8	20

collected before their cutoff time when they commenced the operational analysis. Assimilated data are geopotential height at 1000 hPa, wind and temperature at 10 standard levels below 100 hPa, and relative humidity at six standard levels below 300 hPa. Geopotential height data at the other levels are not assimilated because they are not independent of temperature, moisture, and 1000-hPa geopotential height data. Since the model top is placed at $\sigma = 0.1$, upper-air data above 100 hPa are also not assimilated.

The observation error standard deviations used in the experiments are given in Table 1. They are almost the same as those used in the NCEP operational 3D-VAR system. The observation error standard deviations at 1000, 700, 500, 300, and 100 hPa, except for the geopotential height, are taken from Table 1 of Parrish and Derber (1992), and those at the other levels are calculated by applying a spline interpolation in the logarithm of pressure. The observation error standard deviation of geopotential height at 1000 hPa is taken from Table 5 of Dey and Morone (1985). Observation errors in the radiosonde and pibal data are assumed to be independent of each other, so that the observation error covariance matrix for these data is diagonal. The observation operators for the data consist of inverse spectral transforms to go from spectral to gridpoint representation, conversions from model state variables to observed variables, bicubic horizontal interpolation from model Gaussian grid points to observation points, and cubic vertical interpolations from model sigma levels to observation levels.

A simple quality control procedure is applied to the radiosonde and pibal data by using the NCEP operational analyses at the beginning and end of the assimilation window. The operational analyses are prepared on a $2.5^\circ \times 2.5^\circ$ latitude–longitude grid at the 15 standard pressure levels. The analyses are linearly interpolated to observation times, and then bicubic horizontal interpolation is performed from analysis grid points to observation points. If the magnitude of the difference between an observational datum and interpolated objective analysis is greater than twice the observation error, the observational datum is rejected. Table 2 summarizes the numbers of reported data and rejected data. Zonal and meridional components of the wind are rejected separately in the present study, although this procedure may not be adequate for quality control of radiosonde and pibal wind data. Rejection rates for wind and temperature data are about 5%. The small rejection rate for relative humidity data is due to the use of a relatively large observation error standard deviation. The total number of radiosonde and pibal data that are assimilated in the 4D-VAR experiments during the 12-h assimilation window is 32 681. Since this number is much less than the degrees of freedom in the model, 86 879, the minimization problem is underdetermined. The inclusion of the penalty term in the cost function restricts possible solutions and alleviates this underdeterminancy. Figure 1 displays the horizontal distribution of radiosonde and pibal stations from which data are assimilated in the experiments. The radiosonde and pibal stations are densely distributed over land in the Northern Hemisphere, while they are very sparse over the tropical oceans except for the western tropical Pacific.

b. SSM/I precipitation rates

The SSM/I is a passive microwave radiometer operating on several DMSP satellites since 1987. Their passes cover each earth location twice per day. Two DMSP satellites, *F-10* and *F-11*, were in orbit during the assimilation window of 0000–1200 UTC 22 August 1992. The SSM/I has four channels with frequencies of 19.35, 22.235, 37.0, and 85.5 GHz with nadir horizontal resolution of 15–60 km depending on the frequencies. All measurements except for the 22-GHz channels are obtained with dual polarization. The addition of the 85-GHz channel makes the SSM/I unique in comparison to previous passive microwave instruments. This chan-

TABLE 2. Numbers of reported radiosonde and pibal data with the numbers of rejected data in parentheses.

Time	Geopotential height at 1000 hPa	Zonal wind	Meridional wind	Temperature	Relative humidity
0000–0300 UTC	403 (60)	3546 (214)	3546 (157)	3679 (166)	2097 (39)
0300–0900 UTC	28 (5)	225 (21)	225 (19)	228 (12)	133 (2)
0900–1200 UTC	604 (131)	5429 (342)	5429 (293)	5648 (224)	3200 (54)
Total	1035 (196)	9200 (577)	9200 (469)	9555 (402)	5430 (95)
Rejection rate	18.9%	6.3%	5.1%	4.2%	1.7%

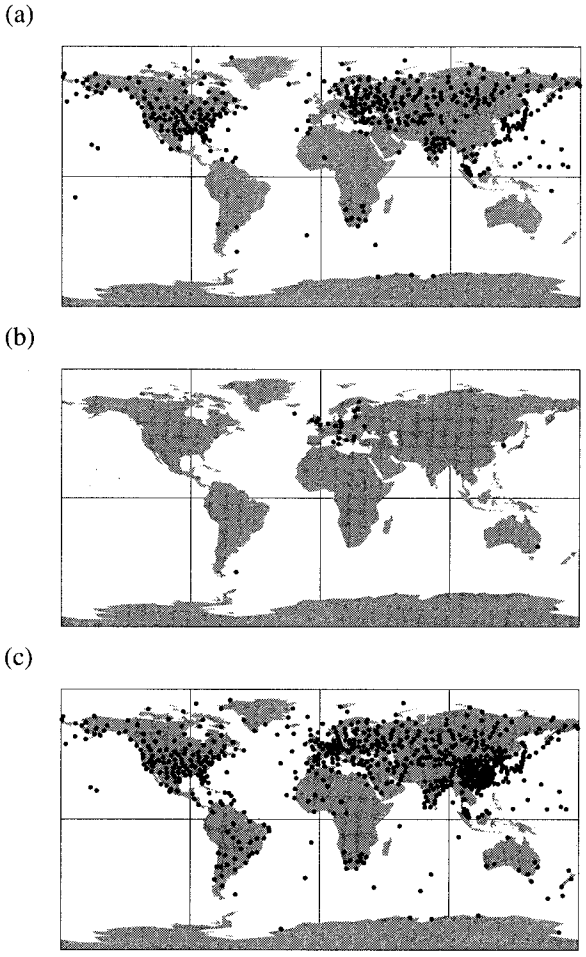

FIG. 1. Horizontal distribution of radiosonde and pibal stations for (a) 0000–0300, (b) 0300–0900, and (c) 0900–1200 UTC 22 August 1992.

nel provides the highest sensitivity for measuring precipitation over land. A conical electrical scan sweeps out a 1400-km swath aft of the satellite. The details of the SSM/I are described in Hollinger et al. (1987).

The SSM/I precipitation rates over the tropical oceans are obtained from the regression formula developed by Olson et al. (1990). This algorithm has been used by Krishnamurti et al. (1993, 1995) for their physical initialization procedure. The algorithm for precipitation over ocean is as follows: if

$$-11.7939 - 0.02727T_B^{37V} + 0.09920T_B^{37H} > 0, \quad (6)$$

then

$$\begin{aligned} R = \max[&\exp(3.06231 - 0.0056036T_B^{85V} \\ &+ 0.0029478T_B^{85H} - 0.0018119T_B^{37V} \\ &- 0.00750T_B^{22V} + 0.0097550T_B^{19V}) \\ &- 8.0, 0], \end{aligned} \quad (7)$$

elsewhere

$$R = 0, \quad (8)$$

where R (mm h^{-1}) is the precipitation rate and T_B (K) the brightness temperature. The superscripts 85, 37, 22, and 19 refer to frequencies (GHz), and the superscripts H and V refer to horizontal and vertical polarizations. A total of 1365 collocated SSM/I and tropical radar measurements over ocean were used to obtain the above regression formula. The bias and the root-mean-square error (rmse) of the precipitation rate estimate are 0.13 mm h^{-1} and 0.59 mm h^{-1}, respectively. The correlation coefficient between the SSM/I measurement and the radar measurement is 0.772. Gairola and Krishnamurti (1992) found a close agreement between rain gauge–based precipitation at island stations and SSM/I-based oceanic precipitation derived from the above algorithm. Olson et al. (1990) also proposed regression formulas for retrieval of precipitation rates over land. Gairola and Krishnamurti (1992) found that over land areas the SSM/I precipitation derived from the Olson algorithm showed large departures from rain gauge measurements. Therefore, SSM/I precipitation rates over land are not assimilated in the present study.

The SSM/I precipitation rates are gridded to a 1° × 1° mesh over ocean between 35°N and 35°S by taking an area average. Since model precipitation is computed on a Gaussian grid with an approximate horizontal resolution of 2.8125° × 2.8125°, an area average over a Gaussian grid box appears more appropriate. However, data coverage of the SSM/I precipitation rates is so limited that an area average over a larger domain may dilute the information carried by the original estimates from the Olson algorithm. The 12-h assimilation window is divided into 12 1-h intervals. The SSM/I estimates of instantaneous precipitation rates belonging to one of the intervals are regarded as hourly mean precipitation rates over this 1-h interval. Bicubic interpolation is applied to interpolate model precipitation rates from model grid points to observation points. In view of the fact that model precipitation rates are computed in physical space not spectral space, bilinear interpolation might appear more appropriate. Results from an assimilation experiment using bilinear interpolation, which will be described in section 4b, suggest otherwise. A quality control procedure is not applied, nor is the bias in the Olson algorithm corrected.

As mentioned in Part II, one of the advantages of 4D-VAR over physical initialization in assimilating precipitation data is the proper treatment of precipitation data error in 4D-VAR. However, assigning observation error standard deviation for precipitation rates is not easy, primarily because of the skewed probability distribution for precipitation rates. The necessity of transforming the precipitation rates to make the observation error more normally distributed was pointed out in Part I. In the present study such transformations are not applied and a constant observation error standard deviation is used for the sake of simplicity. Taking the area av-

erage of the SSM/I precipitation rates over the $1° \times 1°$ grid box reduces the rmse of the original SSM/I estimates from the Olson algorithm. On the other hand, representativeness error should be added to the observation error because the horizontal resolution of model precipitation rates is much larger than that of the SSM/I precipitation rates. There is another error that results from regarding instantaneous precipitation rates as hourly mean precipitation rates. In the present study the observation error standard deviation of the SSM/I precipitation rates is set to 1 mm h^{-1} as a crude estimate. Observation errors in the SSM/I precipitation rates are fundamentally correlated because it is the same sensing device that is acting. However, the observation errors are assumed to be horizontally uncorrelated for simplicity. Thus, the observation error covariance matrix for the precipitation data is also diagonal. The total number of the SSM/I precipitation rates available over the assimilation window is about 2×10^4, so the minimization problem is still underdetermined even if the precipitation data are assimilated. Since the radiosonde and pibal data and the SSM/I precipitation rates are independent of each other, the entire observation error correlation matrix $\mathbf{O}$ in (3) is also diagonal.

Figure 2 shows the SSM/I precipitation rates for four 1-h periods in the assimilation window. The end of the assimilation window is set to 0 h in this figure and Figs. 3, 11, and 13. It is seen that almost the same regions are observed twice by the two DMSP satellites. For example, a region of heavy precipitation in the equatorial Indian ocean was observed during the periods 0000–0100 UTC and 0400–0500 UTC (Figs. 2a and 2b). Regions of heavy precipitation east of New Guinea were observed during the periods 0600–0700 UTC and 1000–1100 UTC (Figs. 2c and 2d). Figure 3 shows the composite of the SSM/I precipitation rates over the assimilation window. Mean values are plotted in areas where more than one observation is available. For later convenience, only the latitudinal belt between 30°N and 30°S is displayed. It is seen that the SSM/I observations do not fully cover the tropical oceans despite the fact that two DMSP satellites are in orbit and that a 12-h assimilation window is taken. About one-third of the tropical oceans remain unobserved. In this period there are no strong tropical disturbances over the tropical oceans except for Hurricane Andrew in the western Atlantic. A small region of precipitation at 25°N, 70°W adjacent to a data-void region is associated with this compact tropical cyclone. Unfortunately the center of the hurricane is not observed by the DMSP satellites during the assimilation window. However, even if the SSM/I observations covered the entire region, the horizontal scale of Hurricane Andrew is too small to be properly resolved by the T42L12 global spectral model. A region of heavy precipitation around 5°N, 165°E is associated with a tropical depression that is developing into Supertyphoon Omar.

Outgoing longwave radiation (OLR) data obtained from the infrared radiometer aboard polar-orbiting satellites have more data coverage in the Tropics, although the OLR data have a poorer physical basis for estimating precipitation rates. Figure 4 displays the night pass and day pass composites of OLR for 22 August 1992. These composites are prepared on a $2.5° \times 2.5°$ grid by the National Environmental Satellite, Data, and Information Service (NESDIS) from measurements by the *NOAA-11* and *NOAA-12* satellites. Equator crossings of the two satellites are at 0230 local time (LT) and 0730 LT for night pass and at 1430 and 1930 LT for day pass, respectively. Thus, OLR data used for the night pass composite in the Atlantic region approximately between 70°W and 40°E and OLR data used for the day pass composite in the Pacific region approximately between 110°E and 180° fall into the assimilation window of 0000–1200 UTC 22 August 1992. The OLR composites in these two regions can be compared with the SSM/I composite in Fig. 3. A close agreement between the SSM/I composite and the OLR composites in the regions suggests that the OLR composites can be used to qualitatively verify the precipitation analysis in SSM/I data-void areas.

4. Results

a. Gradient calculation

The validity of gradient calculation was examined in Part II using the reduced-physics forward model consistent with the adjoint model. Since the forward model and the adjoint model in the present study are not consistent with each other, the adjoint model does not provide the exact gradient of the cost function but yields an approximate gradient. The precision of the approximation can be examined by using the following function:

$$\varphi(\alpha) \equiv \frac{J(\mathbf{x}_0) - J(\mathbf{x}_0 - \alpha \mathbf{S}^2 \tilde{\nabla}_{\mathbf{x}_0} J)}{\alpha (\tilde{\nabla}_{\mathbf{x}_0} J)^{\mathrm{T}} \mathbf{S}^2 \tilde{\nabla}_{\mathbf{x}_0} J}, \tag{9}$$

where α is a small nondimensional parameter and $\mathbf{S}$ is a scaling matrix. The scaling matrix is a diagonal matrix, its diagonal elements consisting of the scaling factors introduced at the end of section 2. The $\tilde{\nabla}_{x_0} J$ is an approximate gradient obtained from backward integration of the inconsistent adjoint model. If the approximate gradient is exact, the value of $\varphi(\alpha)$ should be close to unity for sufficiently small α.

The variations of $\varphi(\alpha)$ with $\log\alpha$ for NOMP and MP are plotted in Fig. 5. The initial guess used in the experiments is taken as $\mathbf{x}_0$. Thus, this figure shows the precision of the gradient calculation at iteration 0 in the minimization process. The penalty parameter r is set to 8×10^{20} s^4. Large values of $\varphi(\alpha)$ for $\alpha = 10^{-12}$ result from numerical cancellation error, so they are to be neglected. It is seen that $\varphi(\alpha)$ is sufficiently close to unity for α less than 10^{-3} for both NOMP and MP. The approximate gradients computed from the inconsistent ad-

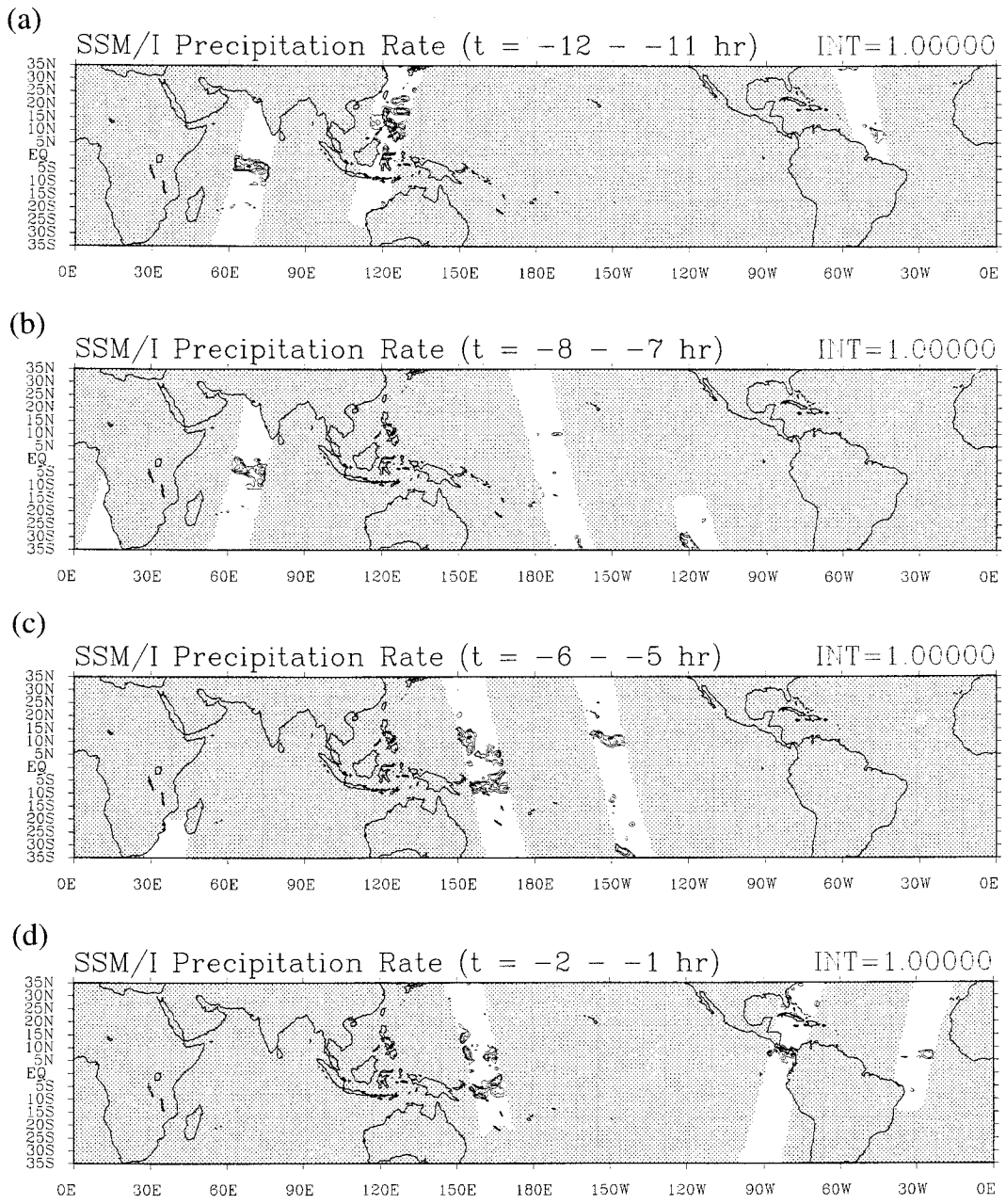

FIG. 2. SSM/I precipitation rates for (a) 0000–0100, (b) 0400–0500, (c) 0600–0700, and (d) 1000–1100 UTC 22 August 1992. Contour intervals are 0.25, 0.5, 1, 2, and 4 mm h^{-1}. Data-void areas are shaded.

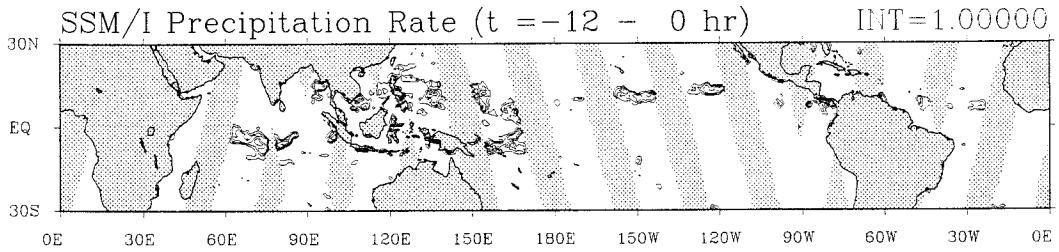

FIG. 3. Composite of SSM/I precipitation rates for 0000–1200 UTC 22 August 1992. Contour intervals are 0.25, 0.5, 1, 2, and 4 mm h^{-1}. Data-void areas are shaded.

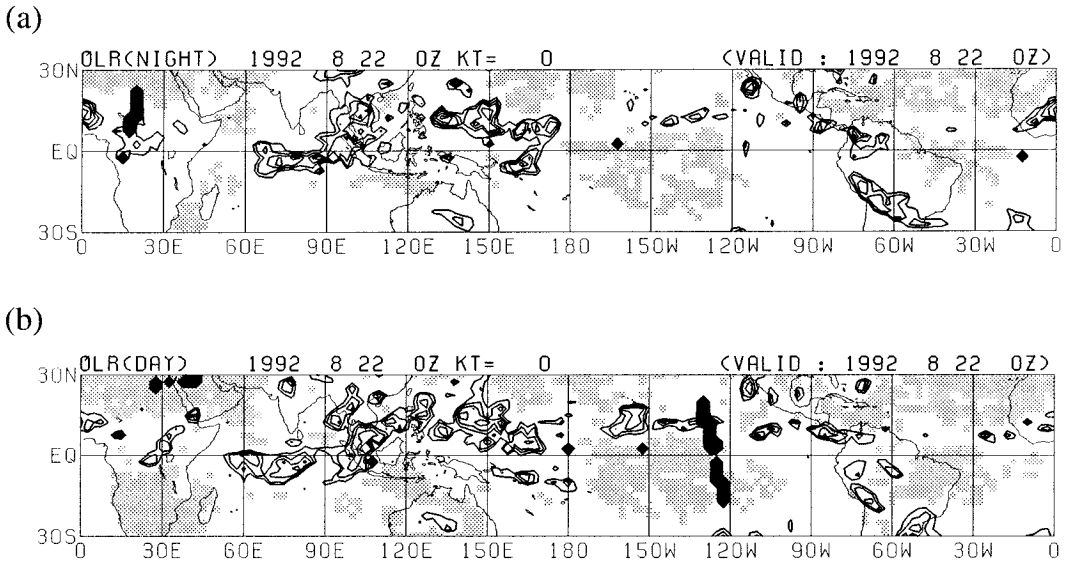

FIG. 4. Composites of outgoing longwave radiation for (a) night pass and (b) day pass of NOAA satellites for 22 August 1992. Contour interval is 25 W m^{-2} and contours greater than 200 W m^{-2} are omitted. Areas of greater than 275 W m^{-2} are lightly shaded. Data-void areas are densely shaded.

joint model appear to have enough precision. Note that $\varphi(\alpha)$ is less than unity for almost all values of α for both methods, indicating that the calculated gradients tend to be slightly overestimated. Unexpectedly, $\varphi(\alpha)$ for NOMP is slightly closer to unity than $\varphi(\alpha)$ for MP. Since the directions of the gradients computed from the two methods are not the same, this does not necessarily mean that the adjoint model without the moist processes generates a more precise gradient than the adjoint model with the moist processes included. However, this result may be partly due to less validity of tangent linear approximation for MP. Part II showed that the range of α in which tangent linear approximation is valid for MP is much smaller than the range of α for NOMP.

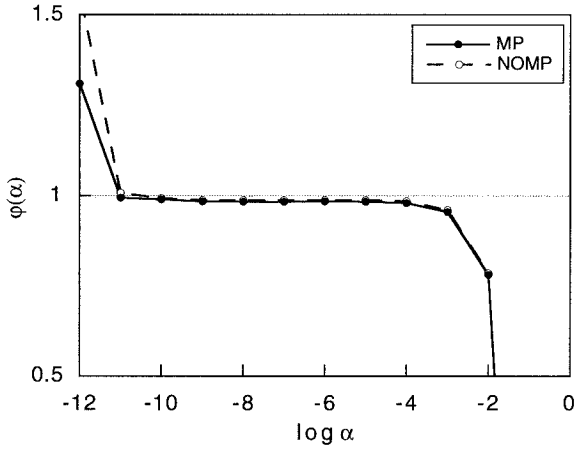

FIG. 5. Variations of the function $\varphi(\alpha)$ with $\log\alpha$ for NOMP and MP with $r = 8 \times 10^{20}$ s^4. The initial guess is taken as $\mathbf{x}_0$.

b. Convergence performance

The cost function and the norm of the scaled approximate gradient are plotted in Fig. 6 as a function of the number of iterations for NOMP, MP, and MP+RR. In the upper panel the upper three lines are the discrepancy terms for radiosonde and pibal data, the middle three lines are the penalty terms, and the lower line is the discrepancy term for precipitation for MP+RR. The parenthetical values in the legend of each panel indicate the number of function calls required for 30 iterations. It is seen that the NOMP method shows slightly better convergence performance than the MP and MP+RR methods. A similar result was obtained in Part II. If the cost function has locally large gradients resulting from highly nonlinear nature of physical processes, a better approximation to the gradient of the cost function does not always leads to better convergence performance because of less validity of the tangent linear approximation. Although the MP and MP+RR methods yield slightly worse fits to the radiosonde and pibal data than the NOMP method, the MP and MP+RR methods produce better precipitation analyses in the Tropics, as will be discussed in the next section. The values of the penalty term remain almost constant during the minimization process for the three methods. Since the initial guess used is the initialized operational analysis, the gravity wave level at iteration 0 may already be at a reasonable level. Therefore, the almost constant penalty terms indicate that the resulting analyses after 30 iterations also have acceptable gravity wave levels. It is to be noted that the approximate gradients of the cost function are not reduced even by an order of magnitude after 30 iterations. Convergence performance will be im-

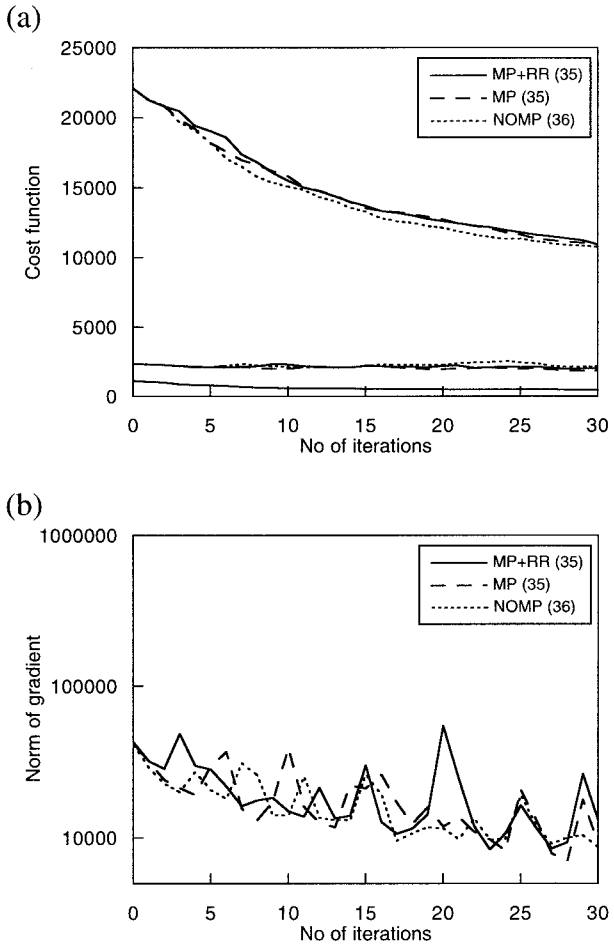

FIG. 6. Variations of (a) the cost function and (b) the scaled approximate gradient of the cost function with the number of iterations for NOMP, MP, and MP+RR with $r = 8 \times 10^{20}$ s^4. In (a) the upper three lines are the discrepancy terms for radiosonde and pibal data, the middle three lines are the penalty terms, and the lower line is the discrepancy term for precipitation data for MP+RR. In (b) the ordinate is on a logarithmic scale. Parenthetical values in the legend of each panel indicate the number of function calls required for 30 iterations.

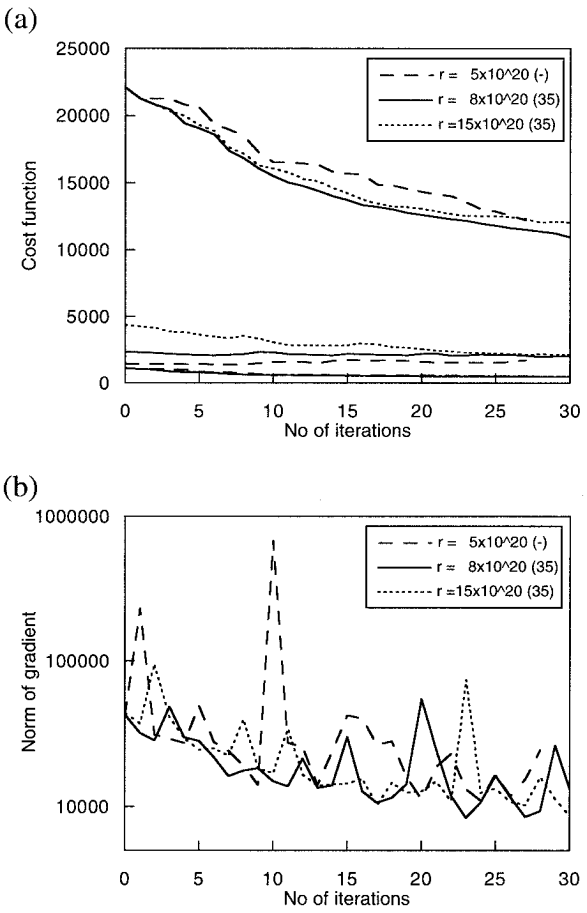

FIG. 7. Same as Fig. 6, except for MP+RR with $r = 5 \times 10^{20}$ s^4, 8×10^{20} s^4, and 15×10^{20} s^4. In (a) the upper three lines are the discrepancy terms for radiosonde and pibal data, the middle three lines are the penalty terms, and the lower three lines are the discrepancy terms for precipitation data.

proved by introducing a preconditioning procedure instead of the simple scaling that is not optimized.

One of the conclusions of Part II is that the penalty term for suppressing gravity wave noise increases the convergence rate of 4D-VAR with the moist processes included by avoiding locally large gradients in the cost function during the minimization process. The sensitivity of convergence performance to the penalty parameter r is shown in Fig. 7 for MP+RR. The cost function and the norm of the scaled approximate gradient are plotted as a function of the number of iterations for the following three penalty parameters: $r = 5 \times 10^{20}$ s^4, 8×10^{20} s^4, and 15×10^{20} s^4. The curves for $r = 8 \times 10^{20}$ s^4 are copied from Fig. 6. Minus signs in the parentheses in the legends indicate that the number of function calls reaches the maximum value, 40, before 30 iterations. It is seen that there is an optimal value of the penalty parameter, $r = 8 \times 10^{20}$ s^4, which gives the best convergence performance. This value also keeps the magnitude of the penalty term almost constant during the minimization process. When $r = 5 \times 10^{20}$ s^4 is used, the convergence is considerably decelerated and the maximum number of function calls is reached before 28 iterations. The lower panel suggests that this deceleration may be primarily caused by excessively large gradients computed by the adjoint model at the first and tenth iterations. This result agrees with results of Part II: too small penalty parameters lead to a poor convergence performance of 4D-VAR with the moist processes included. The penalty term gradually increases during the minimization process, indicating that gravity wave level is too high toward the end of iteration. When $r = 15 \times 10^{20}$ s^4 is used, the convergence performance is also degraded, although large gradients in the cost function are not computed. A decreasing tendency of the penalty term indicates that the gravity wave level is gradually reduced. The excessive suppression of gravity wave level makes it difficult to fit the model solution

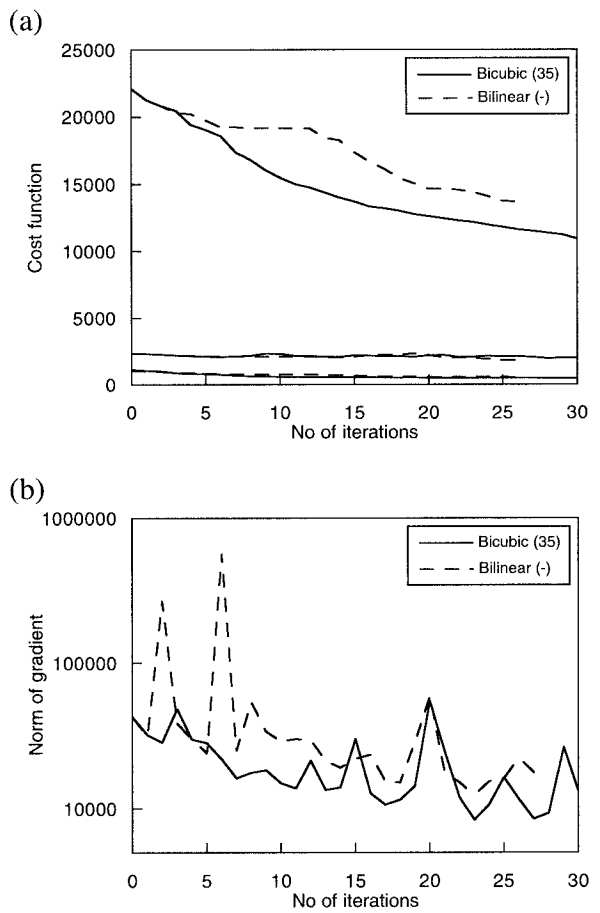

FIG. 8. Same as Fig 6, except for MP+RR with bicubic and bilinear interpolations for precipitation data. In (a) the upper two lines are the discrepancy terms for radiosonde and pibal data, the middle two lines are the penalty terms, and the lower two lines are the discrepancy terms for precipitation data.

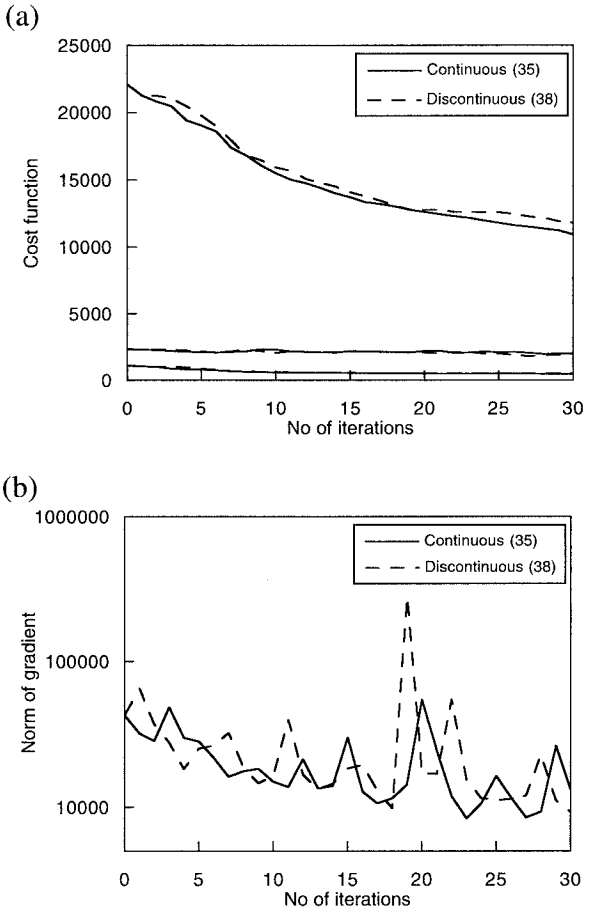

FIG. 9. Same as Fig. 6, except for MP+RR with the continuous and discontinuous moist processes. In (a) the upper two lines are the discrepancy terms for radiosonde and pibal data, the middle two lines are the penalty terms, and the lower two lines are the discrepancy terms for precipitation data.

to the observations and, therefore, decelerates the convergence.

So far in the present study, bicubic interpolation has been used to interpolate model precipitation rates from model grid points to observation points. In view of the fact that model precipitation is calculated in physical space not spectral space and that convective rainfall, which predominates in the Tropics, is a rather localized phenomenon, bilinear interpolation might appear more appropriate. Figure 8 compares convergence performance between bicubic and bilinear interpolations for MP+RR. The penalty parameter r is set to 8×10^{20} s^4. It is seen that the convergence rate is considerably decelerated when bilinear interpolation is used; the maximum number of function calls are reached before 27 iterations. Excessively large gradients are calculated at the second and sixth iterations and may contribute to degradation of the convergence performance. A higher-order interpolator has a smoothing effect on the cost function and, as a result, improves convergence performance.

One of the conclusions of Part I was that variational data assimilation with discontinuous moist processes had poor convergence properties and large analysis errors. However, this conclusion was obtained from the column model assimilation experiments using simulated data. It is interesting to see whether this conclusion holds when using a global primitive equation model and real observations. An assimilation experiment is performed for MP+RR with $r = 8 \times 10^{20}$ s^4 using a discontinuous version of the moist processes. The discontinuous version is the same as that used in Part I. In this version several types of discontinuity such as discontinuous changes in cloud depth and a step-function condition for invoking cumulus convection are not removed from the original parameterization schemes used in the FSU GSM. Figure 9 compares the convergence performance between the discontinuous moist processes and the continuous moist processes that have been used so far in the present study. It is seen that the discontinuous moist processes deteriorate the convergence performance of 4D-VAR. The discontinuous version produces a larger misfit in radiosonde and pibal data and requires three

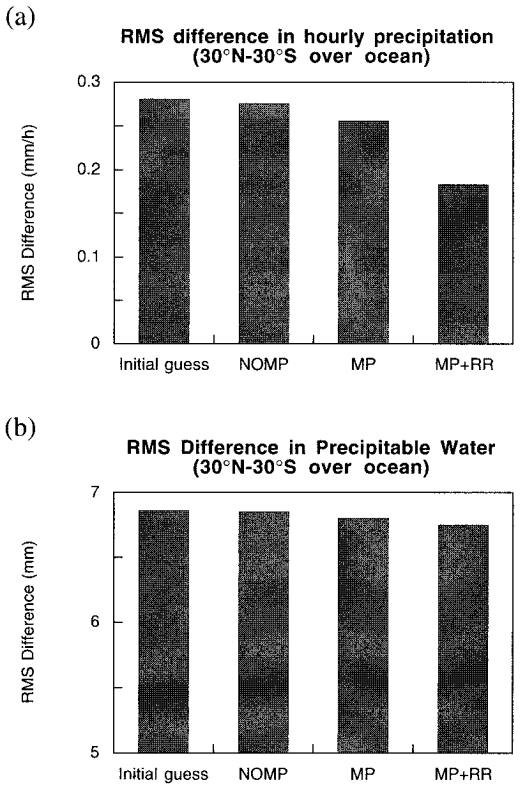

FIG. 10. Root-mean-square differences in (a) hourly mean precipitation rates and (b) precipitable water between the analyses and SSM/I observations over the tropical oceans (30°N–30°S) over the assimilation window.

more function calls for 30 iterations than the continuous version. The misfit in precipitation data is almost the same, but the discontinuous version yields a slightly larger misfit. These results confirm the conclusion of Part I, although differences in convergence performance between the continuous and discontinuous versions are much smaller than differences that may be expected from results of the column model assimilation experiments.

c. Analyzed fields

In this section precipitation and divergence fields in the Tropics after 30 iterations are closely examined for the assimilation experiments presented in Fig. 6. Impacts of the SSM/I precipitation rates on other fields such as vorticity are rather small and, therefore, are not described here. Figure 10a compares misfits in hourly mean precipitation rates for the initial guess and the three assimilation methods over the tropical oceans between 30°N and 30°S where SSM/I data are available. The magnitude of the misfit for NOMP is almost the same as the misfit for the initial guess, indicating that the precipitation analysis is hardly improved when using the adjoint model without the moist processes despite the fact that the full-physics model is used as the forward model. When using the adjoint model with the moist processes included, the misfit is reduced from the initial guess by 9% even without assimilating SSM/I precipitation rates. This result indicates a benefit of including the moist processes in the adjoint model for the tropical data analysis with 4D-VAR. Assimilation of the SSM/I precipitation rates considerably reduces the misfit as may be expected.

Figure 10b shows misfits in precipitable water over the assimilation window. The observed precipitable water is obtained from the SSM/I brightness temperatures using the algorithm developed by Lojou et al. (1994):

$$\begin{aligned} \mathrm{PW} = {} & 20.75 - 2.582 \log(280 - T_B^{19H}) \\ & - 0.3919 \log(280 - T_B^{19V}) \\ & - 3.610 \log(280 - T_B^{22H}) \\ & + 2.729 \log(280 - T_B^{37H}) \\ & - 0.5118 \log(280 - T_B^{37V}), \end{aligned} \tag{10}$$

where PW (g cm^{-2}) is the precipitable water. The brightness temperatures are corrected to eliminate the weak biases observed between the brightness temperature measured by the SSM/I and those computed by the European Centre for Medium-Range Weather Forecasts (ECMWF) model following the method proposed by Lojou et al. (1994). The SSM/I precipitable water is only calculated over the tropical oceans. Similar to the SSM/I precipitation rates used in the experiments, the precipitable water data are prepared on a $1^\circ \times 1^\circ$ grid with a temporal resolution of 1 h. Bicubic interpolation is used to interpolate from model grid points to observation points. It is found that the impact of including the moist processes in the adjoint model and assimilating the SSM/I precipitation rates on the precipitable water analysis is rather small; the misfit for MP+RR is decreased from the initial guess by only 1.5%. A larger impact of assimilating precipitation data on precipitable water analysis was obtained in Part II, where observations of hourly mean precipitation rates were assumed to be available over the entire tropics at every hour. This assumption was too optimistic. Figure 10b strongly suggests the necessity of assimilating the SSM/I precipitable water data to improve the tropical moisture analysis.

Figure 11 compares accumulated precipitations over the 12-h assimilation window produced by the three methods. The corresponding accumulated precipitation obtained from the initial guess is also displayed for comparison. The initial guess precipitation is calculated by making a 12-h prediction with the forward model from the initial guess. In order to evaluate the quality of these precipitation analyses we need observations of 12-h accumulated precipitation over the Tropics, but precipitation observations with sufficient spatial coverage and precision are not available. Here we assume that the spatial pattern of the true accumulated precipitation distribution is not very different from the spatial pattern of the composite of the SSM/I precipitation rates shown in Fig. 3. When using the SSM/I composite for verifi-

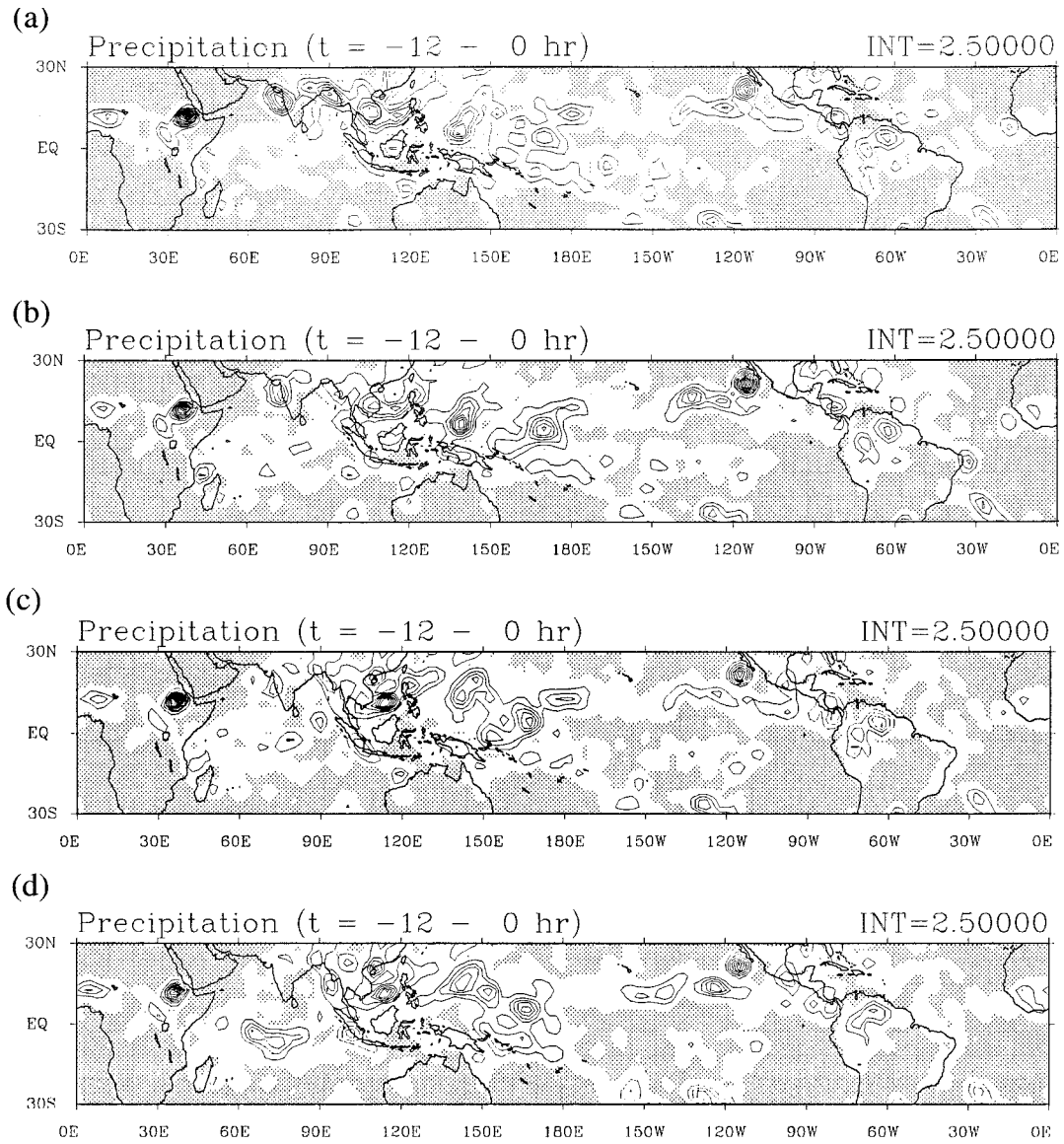

FIG. 11. The 12-h accumulated precipitation over the assimilation window for (a) the initial guess, (b) NOMP, (c) MP, and (d) MP+RR. Contour interval is 2.5 mm. Areas less than 0.25 mm are shaded.

cation purposes, only a qualitative comparison is possible. Since the SSM/I composite is not available over land and data-void regions, the night and day pass composites of OLR shown in Fig. 4 are also used as complementary data in the qualitative verification.

The spatial distribution of the initial guess precipitation (Fig. 11a) exhibits several discrepancies with the spatial distribution of the SSM/I precipitation composite. For example, the initial guess generates heavy precipitation in the eastern Arabian Sea, but the SSM/I composite does not show large precipitation rates in this region. Regions of heavy precipitation over the equatorial Indian Ocean in the SSM/I composite are not seen in the initial guess precipitation. In the tropical Pacific a region of precipitation observed around 10°N, 135°E is misplaced southward by about 10°. A region of precipitation south of the Hawaiian Islands is missing in the initial guess precipitation. The spatial pattern of the precipitation analysis by the NOMP method is almost the same as the spatial pattern of the initial guess precipitation, but precipitation amounts are different in several regions (Fig. 11b). Precipitation around 5°N, 135°E; 5°N, 170°E; and 25°N, 115°W is intensified, while precipitation around the Indian subcontinent is reduced. This result suggests that the adjoint model without moist processes is not adequate to retrieve precipitation in the Tropics even if the full-physics model is used as the forward model.

When using the adjoint model with the moist processes included, significant changes in precipitation analysis are introduced in the western tropical Pacific

(Fig. 11c). The region of heavy precipitation north of New Guinea is shifted northward by about 10°, and the center of heavy precipitation just west of the date line is shifted westward by about 5°. A comparison with the SSM/I precipitation composite in Fig. 3 reveals that the former change makes the spatial pattern of analyzed accumulated precipitation closer to the SSM/I composite. The existence of a SSM/I data-void region around the date line makes it difficult to locate the observed center of the latter heavy precipitation region. This heavy precipitation is associated with a developing tropical depression. The day pass composite of OLR in Fig. 4 is useful for this purpose. As mentioned in section 3b, the day-pass composite of OLR in the western tropical Pacific is produced by using OLR observations in the assimilation window. Consequently, the spatial pattern of the OLR composite in this region is expected to resemble that of the true accumulated precipitation over the assimilation window. The center of low OLR just west of the date line in the day-pass OLR composite is located at 5°N, 165°E (Fig. 4b). Thus, the position of the heavy precipitation produced by the MP method is closer to the observed position than that produced by the NOMP method. There are several radiosonde and pibal stations in the western tropical Pacific in contrast to the other tropical oceans (see Fig. 1). Observational data provided by these stations may contribute to the improved precipitation analysis in the western tropical Pacific. On the other hand, regions of heavy precipitation observed in the equatorial Indian Ocean and south of the Hawaiian Islands are not well retrieved by the MP method, possibly because no radiosonde and pibal data are available in these areas. A point to note here is that if we use the adjoint model without moist processes, radiosonde and pibal data hardly contribute to improvement of precipitation analysis. This result demonstrates the necessity of including the moist processes in the adjoint model for 4D-VAR in the Tropics. A similar conclusion was also obtained in Part II from 4D-VAR experiments in a simulated data framework.

A comparison between Fig. 3 and Fig. 11d reveals that assimilation of the SSM/I precipitation rates with 4D-VAR works quite well. Regions of heavy precipitation in the equatorial Indian Ocean and south of the Hawaiian Islands are well retrieved. Erroneous areas of precipitation over the ocean around western India, northwest of Madagascar, and northwest of Australia are removed. The spatial distribution of the precipitation analysis by the MP+RR method exhibits a closer agreement in the western tropical Pacific with the day pass OLR composite (Fig. 4b) than that of the precipitation analysis by the MP method even in SSM/I data-void areas. Since wind speeds in the Tropics are generally smaller than in the extratropics, significant horizontal advection of information from data available areas to data void areas is not expected when using a 12-h assimilation window. The improvement in the precipitation analysis in SSM/I data-void areas primarily results

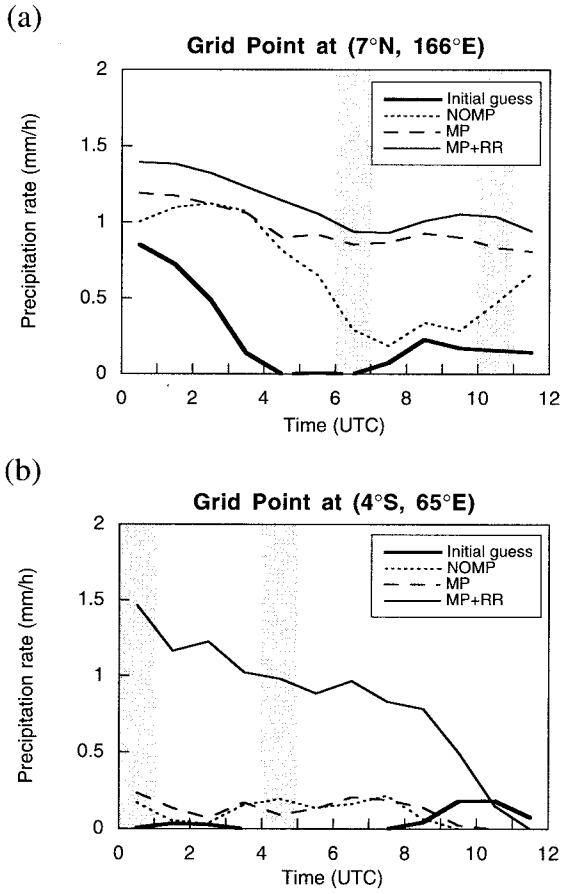

FIG. 12. Time sequences of precipitation rates for the assimilation window at (a) 7°N, 166°E and (b) 4°S, 65°E. The 1-h intervals when SSM/I observations are available are shaded.

from assimilating other observational data by using the full model dynamics. This is one of the advantages of 4D-VAR over physical initialization. In physical initialization some of the model state variables are directly modified so that model precipitation rates are close to observed precipitation rates, but such direct modifications are not performed in regions where precipitation observations are not available. For this reason the existence of data-void areas are undesirable in physical initialization procedures.

The time sequences of hourly mean precipitation rates at two Gaussian grid points at 7°N, 166°E and 4°S, 65°E are shown in Fig. 12. These two points are near the centers of heavy precipitation regions in the precipitation analysis by the MP+RR method (Fig. 11d). The 1-h intervals in which the SSM/I precipitation rates are available are shaded. The horizontal distribution of the SSM/I precipitation rates at these 1-h intervals is displayed in Fig. 2. At the grid point in the western tropical Pacific (Fig. 12a) the precipitation rates for the initial guess and NOMP are much smaller than those for MP and MP+RR. The precipitation rate produced by the MP+RR method is slightly larger than the precipitation

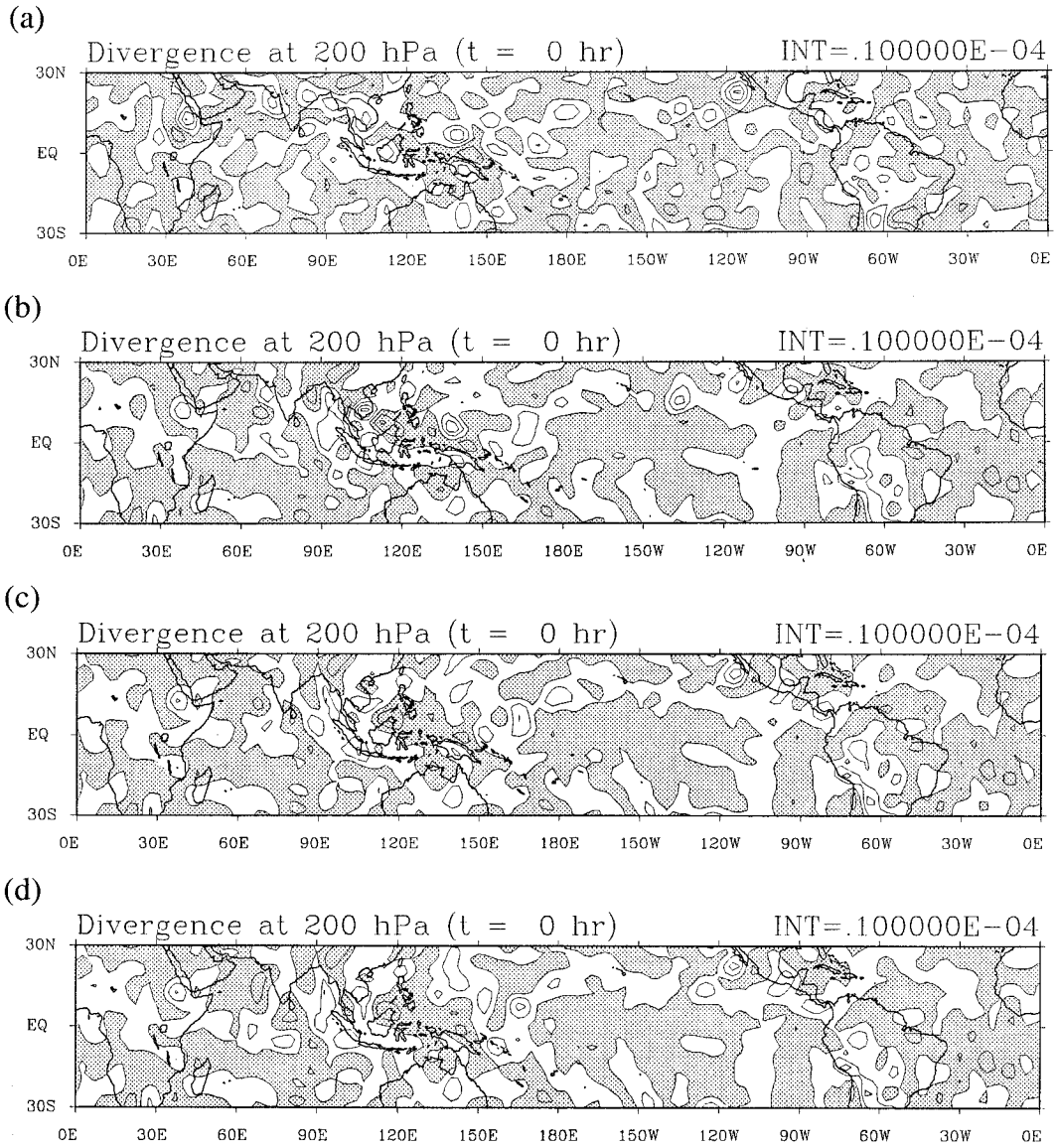

FIG. 13. Divergence at 200 hPa at the end of assimilation window for (a) the initial guess, (b) NOMP, (c) MP, and (d) MP+RR. Contour interval is 1×10^{-5} s^{-1}. Negative areas are shaded.

rate produced by the MP method. In other words, use of the adjoint model with the moist processes included has much more impact on the precipitation analysis at this point than assimilation of the SSM/I precipitation rates. At the grid point in the equatorial Indian Ocean the precipitation rates for the initial guess, NOMP, and MP are much smaller than that for MP+RR (Fig. 12b). Since radiosonde and pibal data are not available around this point, assimilation of the SSM/I precipitation rates is necessary to significantly improve the precipitation analysis. The precipitation analysis by the MP+RR method exhibits a decreasing tendency in the assimilation window. An inspection of Figs. 2a and 2b reveals that the SSM/I precipitation rates around this point also show a decreasing tendency. This time tendency of the observed precipitation rates is reflected in the analyzed precipitation rates. It is also to be noted that the impact of assimilating the SSM/I precipitation rates with 4D-VAR spreads over the whole assimilation window, not just simply around the observation times.

Figure 13 compares analyzed 200-hPa divergence fields at the end of the assimilation window. Divergence in the Tropics is closely related to convective activity. Centers of strong divergence north of New Guinea obtained from the initial guess and the NOMP method are associated with the misplaced heavy precipitation in this region (see Figs. 11a and 11b). Strong divergence west of India obtained from the initial guess is gradually replaced by convergence moving through the NOMP, MP, and MP+RR analyses. In a similar fashion the up-

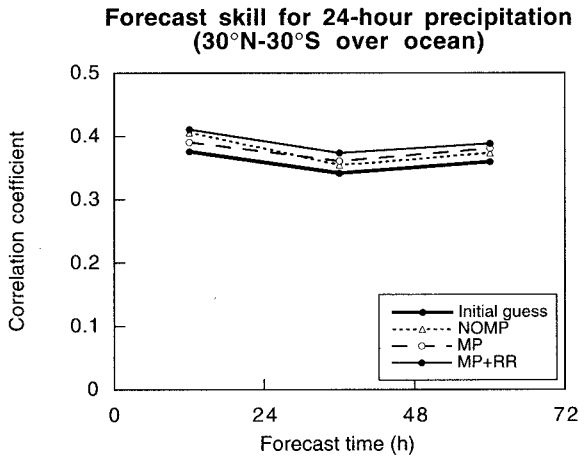

FIG. 14. Forecast skill for 24-h accumulated precipitation over the tropical oceans (30°N–30°S) up to 72 h.

per-level divergence associated with the developing tropical depression around 5°N, 165°E becomes stronger and more compact. A comparison between Figs. 13c and 13d reveals that the impact of assimilating the SSM/I precipitation rates on divergence analysis is not very remarkable. The magnitude of the impact may be highly case dependent. If there is a strong tropical disturbance in a region where conventional observations are not available, much larger impact may be obtained as in the assimilation experiments performed in Part II. In the western Atlantic, possible strong divergence associated with Hurricane Andrew is not retrieved by any of the methods. This may be due to the fact that the spatial resolution of the model is not high enough to resolve this compact tropical cyclone. Note that the divergence fields produced by the three methods are smoother than the divergence field obtained from the initial guess. This may be primarily due to the inclusion of the penalty term in the cost function that suppresses large time tendencies of divergence.

d. Precipitation forecast

The quality of the analyses can also be evaluated by examining the skill of forecasts starting from the analyses. Figure 14 compares forecast skills for 24-h precipitation totals over the tropical oceans between 30°N and 30°S for the initial guess, NOMP, MP, and MP+RR. The problem here is that reliable verification data for the precipitation totals are not available over the verification area. It is assumed, as before, that the spatial pattern of the composites of the SSM/I precipitation rates for 24-h periods are not very different from that of the true 24-h precipitation totals. The correlation coefficient is used to score the forecasts. The SSM/I precipitation rates measured by the two DMSP satellites cover almost all the tropical oceans over 24-h periods. Since the composites are produced from instantaneous precipitation rates, small-scale features that are unlikely in the 24-h precipitation totals are present in the composites. In order to remove these undesirable small-scale features, a moving average over a $5^\circ \times 5^\circ$ domain is applied to the SSM/I precipitation composites.

It is seen from Fig. 14 that the forecast skill up to 72 h tends to increase by including the moist processes in the adjoint model or by assimilating the SSM/I precipitation rates. However, differences in the forecast skill between the initial guess and the three assimilation methods are rather small. One of the reasons for these small differences may be that a background term that possesses the observational information prior to the assimilation window is not included in the cost function. The initial guess for the model state at the beginning of the assimilation window is the NCEP operational analysis at this point. The operational analysis is prepared by using background information as well as observational data. Omitting the background term makes it difficult to utilize this information in the assimilation experiments carried out here. Another reason may be that the number of radiosonde and pibal stations that are assimilated in the experiments is very limited over the tropical oceans.

An unexpected result in Fig. 14 is the better skill of the forecast starting from the NOMP analysis compared to the forecast starting from the MP analysis over the first 24-h interval. As discussed in section 4b, 4D-VAR with the moist processes included has a slightly slower convergence rate than 4D-VAR without the moist processes. The discrepancy term for radiosonde and pibal data for MP is larger than that for NOMP (see Fig. 6a). Although the MP method produces better precipitation and divergence analyses in the Tropics, it is not clear whether the quality of the MP analysis in the Tropics after 30 iterations is better as a whole than the quality of the NOMP analysis after the same number of iterations.

The small impact of assimilating the SSM/I precipitation rates on the precipitation forecast skill even over the first 24-h interval may be an expected result in view of the small impact on the divergence analysis (see Fig. 13). Assimilation of satellite precipitable water data will improve the moisture analysis in the Tropics and will be helpful to increase the precipitation forecast skill. Another factor to consider is the general inability of the model to well predict synoptic-scale tropical precipitating systems. The assimilation experiments in a simulated data framework performed in Part II demonstrated that the T42L12 FSU GSM is capable of predicting a supertyphoon quite well at least up to 72 h. However, such a large-scale strong tropical precipitating system is absent in the present case, so that a high forecast skill may be hard to obtain even if a good initial condition is prepared. A forecast experiment for the same case was carried out with a T213 version of the FSU GSM by Krishnamurti et al. (1995) using their physical initialization procedure. Their results showed that the high-resolution model succeeded in simulating the developing stage of the tropical depression located around 5°N, 165°E. In contrast, this weak tropical disturbance

gradually decays in the forecast experiment performed here with the T42 version of the FSU GSM (not shown).

5. Conclusions

The conclusions of this paper are as follows.

- The following three procedures improve the convergence performance of 4D-VAR using the adjoint model with the moist processes included: appropriate control of gravity wave level, removal of discontinuities from parameterization schemes of the moist processes, and use of a higher-order horizontal interpolation operator for precipitation when assimilating precipitation data.
- 4D-VAR using the adjoint model that lacks the moist processes produces a poor analysis in the Tropics despite the fact that the full-physics model is used as the forward model. Inclusion of the moist processes in the adjoint model yields a better precipitation analysis even without assimilating the SSM/I precipitation rates, especially in areas where several radiosonde and pibal observations are available. However, the convergence rate is slightly decelerated by including the moist processes.
- The impact of assimilating the SSM/I precipitation rates on the precipitation analysis is not confined to around SSM/I observation times but spreads over the whole assimilation window. Its impact on the precipitable water analysis over the tropical oceans is positive but very small, suggesting the necessity of assimilating satellite precipitable water data. Assimilation of the SSM/I precipitation rates slightly improves the precipitation forecast over the tropical oceans.

These conclusions are generally in agreement with conclusions of Part I and Part II. However, they are derived from a case study and assimilation experiments for other cases are highly desirable. It should be emphasized that inclusion of the moist processes in the adjoint model is necessary for a better tropical data assimilation with 4D-VAR, even if the full-physics model is used as the forward model or precipitation data are not assimilated. A problem introduced by including the moist processes in the adjoint model is the slight degradation in the convergence performance due to less validity of tangent linear approximation. Additional smoothing of the moist processes, especially parameterization schemes for deep cumulus convection, will probably improve the convergence performance of 4D-VAR with moist processes included. Introduction of preconditioning is also desirable for this purpose.

One of the deficiencies of the present study is that a background term is not included in the cost function. Inclusion of a background term may possibly improve the impact of SSM/I precipitation rates on precipitation forecast, since much more information is available in data assimilation. It is to be noted that a background term with multivariate balance conditions is helpful to control gravity wave level. Keeping gravity wave activity at an appropriate level during the minimization process is important for faster convergence of 4D-VAR in the Tropics. Use of a higher-resolution model will also increase the impact of the SSM/I precipitation data through better ability of the model to simulate tropical precipitating disturbances.

The results of this study suggest that 4D-VAR can provide a reliable estimate of precipitation over the global Tropics. No single technique exists for reliably estimating global precipitation. Rain gauges provide relatively accurate measurements at a specific point, but area averages derived from gauge observations suffer from severe limitations due to sampling problems. Rain radars observe a relatively large area of 200–300 km in radius, but the spatial distribution of radar data is generally limited to populated land areas. Satellite IR estimates from geosynchronous platforms have a poorer physical basis for estimating precipitation. Satellite microwave estimates have a better physical basis, but they are only available a few times per day from polar-orbiting platforms. Short-range prediction by NWP models can provide precipitation estimates with complete global coverage by using physical laws and observed initial conditions, but the quality of model precipitation is limited by errors in models and initial conditions. Objective techniques that combine the useful portions of available estimates are desirable to improve estimates of global precipitation. Huffman et al. (1995) proposed a technique to combine precipitation estimates from satellite microwave data, satellite IR data, rain gauge data, and short-range prediction from a NWP model. 4D-VAR utilizes the model dynamics and observations in the assimilation window in an optimal way to produce global precipitation estimates. Although precipitation estimates derived from 4D-VAR are still not free from model error, the present study demonstrates the ability of 4D-VAR to provide a reliable estimate of accumulated precipitation over the Tropics.

In the forthcoming Tropical Rainfall Measuring Mission (TRMM) project, a rain radar aboard a satellite in a nonsunsynchronous orbit will provide more accurate precipitation estimates over the global Tropics than microwave estimates (Theon and Fugono 1988). 4D-VAR can easily assimilate TRMM precipitation data along with other available observational data, including other satellite precipitation and precipitable water estimates. It can also produce dynamically consistent estimates of related fields such as condensational heating rates by using model dynamics. Thus, application of 4D-VAR to assimilate TRMM data may be the most promising approach to accomplishing one of the goals of the TRMM project, that is, a reliable estimate of precipitation and latent heating over the global Tropics.

Acknowledgments. This research was done during the author's visit to the Florida State University. The author is sincerely thankful to Prof. T. N. Krishnamurti for providing the opportunity for the visit. It is a pleasure

to thank Drs. A. da Silva, A. Kasahara, I. M. Navon, X. Zou, D. Zupanski, and M. Zupanski for helpful discussions. Special thanks go to Mr. R. Treadon for correcting the English errors in the manuscript. This research was supported by NSF Grant ATM 9312537 and NASA Grants NAG 8-914 and NAG 5-1595. The computations for this work were carried out on the CRAY-C90 at San Diego Supercomputer Center.

REFERENCES

Adler, R. F., and A. J. Negri, 1988: A satellite infrared technique to estimate tropical convective and stratiform rainfall. *J. Appl. Meteor.,* **27,** 30–51.

——, H.-Y. M. Yeh, N. Prasad, W.-K. Tao, and J. Simpson, 1991: Microwave simulations of a tropical rainfall system with a three-dimensional cloud model. *J. Appl. Meteor.,* **30,** 924–953.

Andersson, E., J. Pailleux, J.-N. Thépaut, J. R. Eyre, A. P. McNally, G. A. Kelly, and P. Courtier, 1994: Use of cloud-clear radiances in three/four-dimensional variational data assimilation. *Quart. J. Roy. Meteor. Soc.,* **120,** 627–653.

Arkin, P. A., and B. N. Meisner, 1987: The relationship between large-scale convective rainfall and cloud over the Western Hemisphere during 1982–1984. *Mon. Wea. Rev.,* **115,** 51–74.

Berg, W., and R. Chase, 1992: Determination of mean rainfall from the Special Sensor Microwave/Imager (SSM/I) using a mixed lognormal distribution. *J. Atmos. Oceanic Technol.,* **9,** 129–141.

Businger, J. A., J. C. Wyngard, Y. Izumi, and E. F. Bradley, 1971: Flux profile relationship in the atmospheric surface layer. *J. Atmos. Sci.,* **28,** 181–189.

Chang, C. B., 1979: On the influences of solar radiation and diurnal variation of surface temperatures on African disturbances. FSU Rep. 79-3, 157 pp. [Available from Department of Meteorology, The Florida State University, Tallahassee, FL 32306.]

Dey, C. H., and L. L. Morone, 1985: Evolution of the National Meteorological Center global data assimilation system: January 1982–December 1983. *Mon. Wea. Rev.,* **113,** 304–318.

Gairola, R. K., and T. N. Krishnamurti, 1992: Rain rates based on SSM/I, OLR and raingauge data sets. *Meteor. Atmos. Phys.,* **50,** 165–174.

Grody, N. C., 1991: Classification of snow cover and precipitation using the Special Sensor Microwave Imager. *J. Geophys. Res.,* **96,** 7423–7435.

Hollinger, J., R. Lo, G. Poe, R. Savage, and J. Pierce, 1987: Special Sensor Microwave/Imager user's guide. Naval Research Laboratory, 120 pp. [Available from Naval Research Laboratory, Washington, DC 20375.]

Holton, J. R., 1992: *An Introduction to Dynamic Meteorology.* 3d ed. Academic Press, 511 pp.

Huffman, G. J., R. F. Adler, B. Rudolf, and U. Schneider, 1995: Global precipitation estimates based on a technique for combining satellite-based estimates, rain gauge analysis, and NWP model precipitation information. *J. Climate,* **8,** 1284–1295.

Kidd, C., and E. C. Barrett, 1990: The use of passive microwave imagery in rainfall monitoring. *Remote Sens. Rev.,* **4,** 415–450.

Kitade, T., 1983: Nonlinear normal mode initialization with physics. *Mon. Wea. Rev.,* **111,** 2194–2213.

Krishnamurti, T. N., S. Low-Nam, and R. Pasch, 1983: Cumulus parameterization and rainfall rates II. *Mon. Wea. Rev.,* **111,** 815–828.

——, K. Ingles, S. Cocke, R. Pasch, and T. Kitade, 1984: Details of low latitude medium-range numerical weather prediction using a global spectra model, Part II, Effect of orography and physical initialization. *J. Meteor. Soc. Japan,* **62,** 613–649.

——, H. S. Bedi, and K. Ingles, 1993: Physical initialization using SSM/I rain rates. *Tellus,* **45A,** 247–269.

——, S. K. R. Bhowmik, D. Oosterhof, G. Rohaly, and N. Surgi, 1995: Mesoscale signatures within the tropics generated by physical initialization. *Mon. Wea. Rev.,* **123,** 2771–2790.

Kummerow, C., and L. Giglio, 1994a: A passive technique for estimating rainfall and vertical structure information from space. Part I: Algorithm description. *J. Appl. Meteor.,* **33,** 3–18.

——, and ——, 1994b: A passive technique for estimating rainfall and vertical structure information from space. Part II: Applications to SSM/I data. *J. Appl. Meteor.,* **33,** 19–34.

Liu, D. C., and J. Nocedal, 1989: On the limited memory BFGS method for large scale optimization. *Math. Programming,* **45,** 503–528.

Liu, G., and J. A. Curry, 1992: Retrieval of precipitation from satellite microwave measurement using both emission and scattering. *J. Geophys. Res.,* **97,** 9959–9974.

Lojou, J.-Y., R. Bernard, and L. Eymard, 1994: A simple method for testing brightness temperatures from satellite microwave radiometers. *J. Atmos. Oceanic Technol.,* **11,** 387–400.

Louis, J. F., 1979: A parametric model of vertical eddy fluxes in the atmosphere. *Bound.-Layer Meteor.,* **17,** 187–202.

Olson, W. S., 1989: Physical retrieval of rain rates over the ocean by multispectral microwave radiometry: Application to tropical cyclones. *J. Geophys. Res.,* **94,** 2267–2279.

——, F. J. LaFontaine, W. L. Smith, and T. H. Achtor, 1990: Recommended algorithms for the retrieval of rainfall rates in the tropics using the SSM/I (DMSP-8). CIMSS/Space Science and Engineering Center, 10 pp. [Available from University of Wisconsin, Madison, WI 53706.]

Parrish, D. F., and J. C. Derber, 1992: The National Meteorological Center's spectral statistical-interpolation analysis system. *Mon. Wea. Rev.,* **120,** 1747–1763.

Pasch, P. J., 1983: On the onset of the planetary scale monsoon. FSU Rep. 83-9, 220 pp. [Available from Department of Meteorology, Florida State University, Tallahassee, FL 32306.]

Petty, G. W., 1994a: Physical retrievals of over-ocean rain rate from multichannel microwave imagery. Part I: Theoretical characteristics of normalized polarization and scattering indices. *Meteor. Atmos. Phys.,* **54,** 79–99.

——, 1994b: Physical retrievals of over-ocean rain rate from multichannel microwave imagery. Part II: Algorithm implementation. *Meteor. Atmos. Phys.,* **54,** 101–121.

Theon, J., and N. Fugono, 1988: *Tropical Rainfall Measurements.* A. Deepak Publishers, 523 pp.

Thépaut, J.-N., R. N. Hoffman, and P. Courtier, 1993a: Interactions of dynamics and observations in a four-dimensional variational assimilation. *Mon. Wea. Rev.,* **121,** 3393–3414.

——, D. Vasiljevic, P. Courtier, and J. Pailleux, 1993b: Variational assimilation of conventional meteorological observations with a multilevel primitive-equation model. *Quart. J. Roy. Meteor. Soc.,* **119,** 153–186.

Tsuyuki, T., 1996a: Variational data assimilation in the Tropics using precipitation data. Part I: Column model. *Meteor. Atmos. Phys.,* **60,** 87–104.

——, 1996b: Variational data assimilation in the Tropics using precipitation data. Part II: 3D model. *Mon. Wea. Rev.,* **124,** 2545–2561.

Wilheit, T. J., A. T. C. Chang, and L. S. Chiu, 1991: Retrieval of monthly rainfall indices from microwave radiometric measurements using probability distribution functions. *J. Atmos. Oceanic Technol.,* **8,** 118–136.

Zou, X., I. M. Navon, and J. Sela, 1993a: Control of gravitational oscillations in variational data assimilation. *Mon. Wea. Rev.,* **121,** 272–289.

——, ——, and ——, 1993b: Variational data assimilation with moist threshold processes using the NMC spectral model. *Tellus,* **45A,** 370–387.

Zupanski, D., 1993: The effects of discontinuities in the Betts–Miller cumulus convection scheme on four-dimensional variational data assimilation. *Tellus,* **45A,** 511–524.

——, and F. Mesinger, 1995: Four-dimensional variational assimilation of precipitation data. *Mon. Wea. Rev.,* **123,** 1112–1127.

Zupanski, M., 1993: Regional four-dimensional variational data assimilation in a quasi-operational forecasting environment. *Mon. Wea. Rev.,* **121,** 2396–2408.